Supplementary Information

An efficient, green, and residual oxidant-free wastewater treatment technology enabled by coupling dual-cathode heterogeneous electro-Fenton and UV radiation in tandem

Lele Cui[a,b,c], Mingming Sun[a,b,c], and Zhenghua Zhang[a,b,c]*

[a]Membrane & Nanotechnology-Enabled Water Treatment Center, Institute of Environment and Ecology, Tsinghua Shenzhen International Graduate School, Tsinghua University, Shenzhen 518055, Guangdong, China

[b]Guangdong Provincial Engineering Research Centre for Urban Water Recycling and Environmental Safety, Tsinghua Shenzhen International Graduate School, Tsinghua University, Shenzhen, 518055, Guangdong, China

[c]School of Environment, Tsinghua University, Beijing 100084, China

Green Chemistry

Submitted May 2023

*Corresponding author: zhenghua.zhang@sz.tsinghua.edu.cn (Z.H. Zhang)

Text S1. Chemicals

Carbon black (CB, Vulcan XC-72), polytetrafluoroethylene (PTFE, 60%), 1,10-phenanthroline ($C_{12}H_8N_2$, 99%), and potassium titanium (IV) oxalate ($K_2TiO(C_2O_4)_2$, ≥98%) were purchased from Shanghai Aladdin Biological Technology Co., Ltd. Anhydrous sodium sulfate (Na_2SO_4, 99%), iron(III) chloride hexahydrate ($FeCl_3 \cdot 6H_2O$, 99%), sodium hydroxide (NaOH, 96%), tert-butyl alcohol (TBA, ≥99%), methanol (MeOH, 99.5%), dimethyl sulfoxide (DMSO, >99.8%), p-benzoquinone (BQ, ≥99%), oxytetracycline (OTC, 95%), tetracycline (TC, ≥98), ranitidine (RNTD, ≥98%), sulfamethoxazole (SMX, 98%), 2,2,6,6-tetramethyl-4-piperidinoland (TEMP, 99%), and 5,5-dimethylpyrroline-1-oxide (DMPO, 97%) were supplied by Shanghai Macklin Biochemical Co., Ltd. Graphite felt (GF, Shanghai Hongjun Industry Co., Ltd.) was used in the preparation of air-diffusion cathode (ADC) and FeOCl/GF catalytic cathode. Ti mesh electrode coated with noble metal Pt was used as the anode material and was bought from Suzhou Shuertai Industrial Technology Co., Ltd.

Text S2. Characterizations

The contact angle of ADC was recorded using a contact angle instrument (Kruss DSA30). The morphology and elemental distribution of ADC and FeOCl/GF was characterized by scanning electron microscopy (SEM) (Tescan Mira4) coupled with X-ray energy dispersive spectroscopy (EDS) (Oxford). The crystalline structures of different materials were analyzed using an X-ray diffractometer (XRD) (Rigaku Ultima IV) with a Cu kα radiation. X-ray photoelectron spectroscopy (XPS) (Thermo Scientific) was used to determine the changes in the relative concentrations of different iron species on the FeOCl/GF surface before and after the reaction.

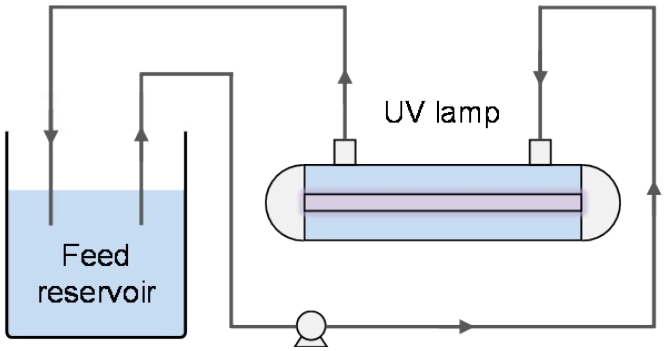

Fig. S1. Schematic illustration of the UV system.

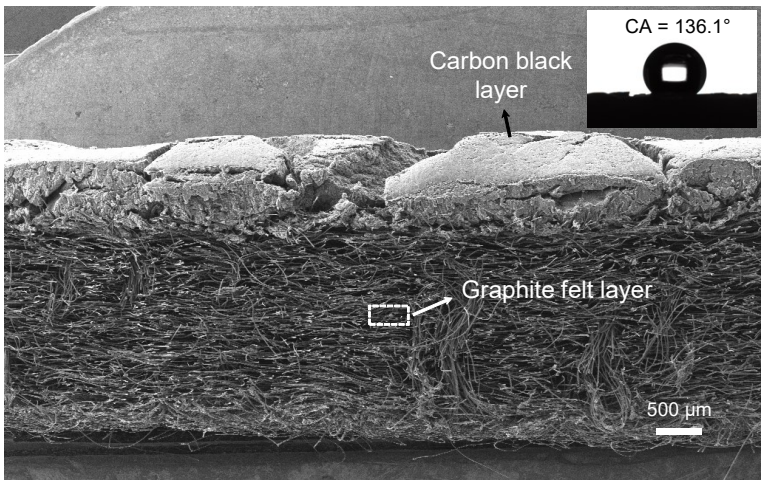

Fig. S2. Cross-sectional SEM image of ADC electrode and contact angle of the catalytic layer (inset).

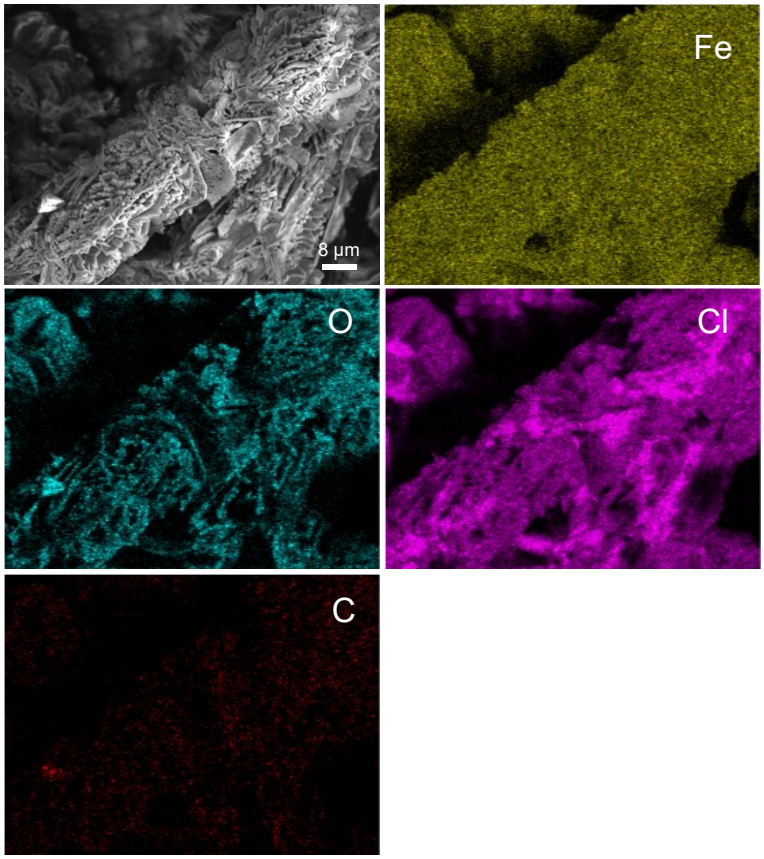

Fig. S3. Fe, O, Cl, and C elemental mapping of the FeOCl/GF catalytic cathode.

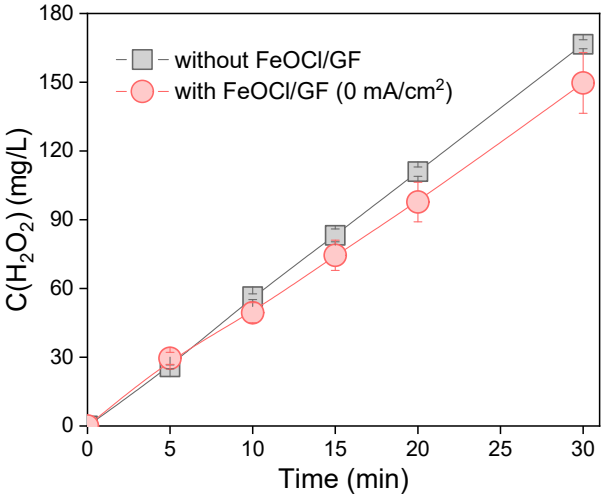

Fig. S4. Comparison of the accumulation concentration of H_2O_2 in the dual-cathode system with no current applied to the FeOCl/GF cathode and the ADC single-cathode system.

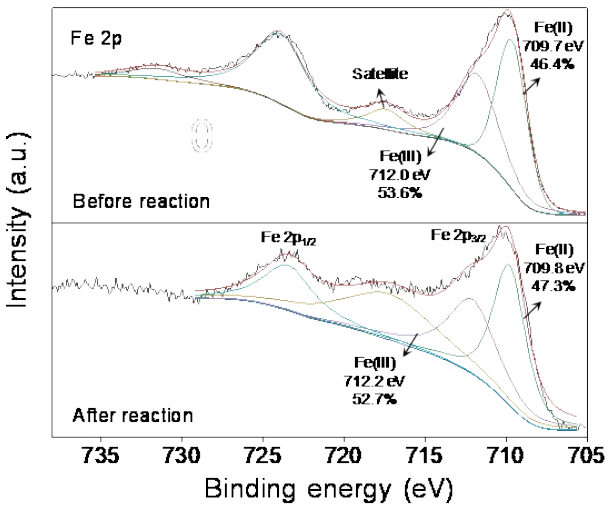

Fig. S5. High-resolution XPS spectra of Fe 2p for FeOCl/GF pre- and post-degradation reaction.

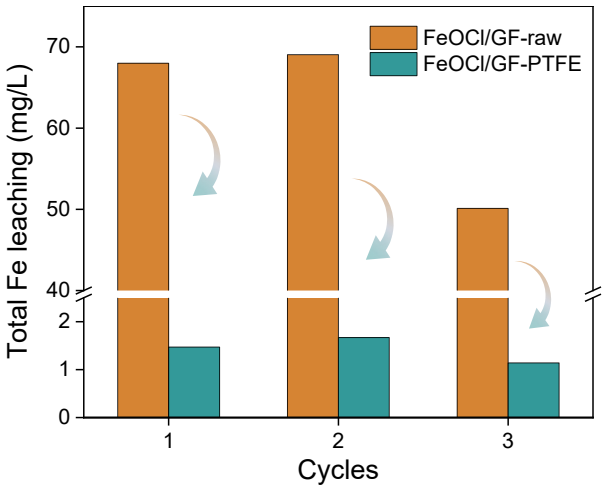

Fig. S6. Comparison of the total Fe leaching of FeOCl/GF catalytic cathode with or without PTFE post-treatment in three runs.

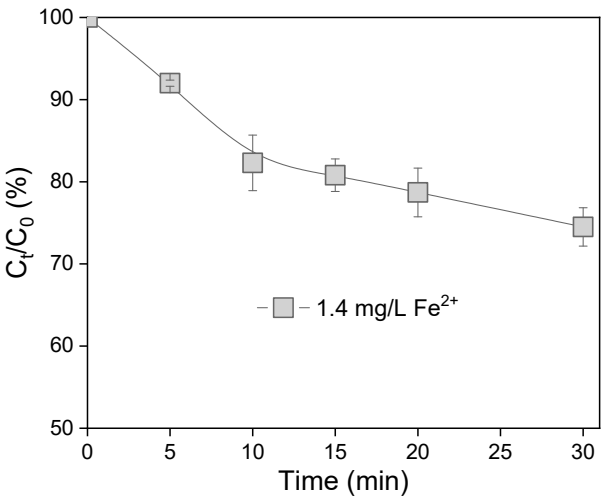

Fig. S7. OTC degradation performance of homogeneous EF driven by Fe^{2+} (1.4 mg/L) leached from FeOCl/GF catalytic cathode (conditions: ADC cathode, Ti/Pt mesh anode, [OTC] = 20 mg/L, pH = 4, and I_{ADC} = 25 mA/cm^2).

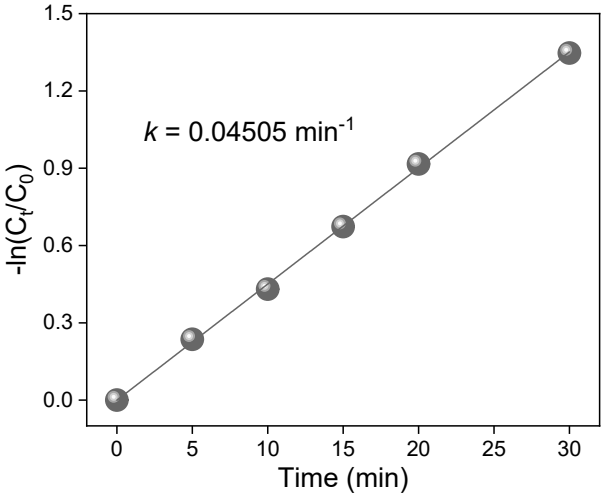

Fig. S8. Apparent reaction kinetic curve for OTC degradation at a current density of 5 mA/cm^2 applied to both ADC and FeOCl/GF cathodes.

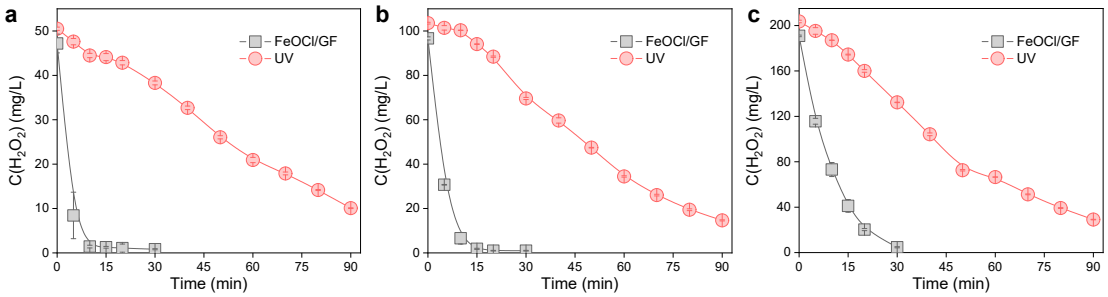

Fig. S9. Comparison of the decomposition rate of H_2O_2 by FeOCl/GF catalytic cathode and UV radiation: (a) ~50 mg/L, (b) ~100 mg/L, and (c) ~200 mg/L.

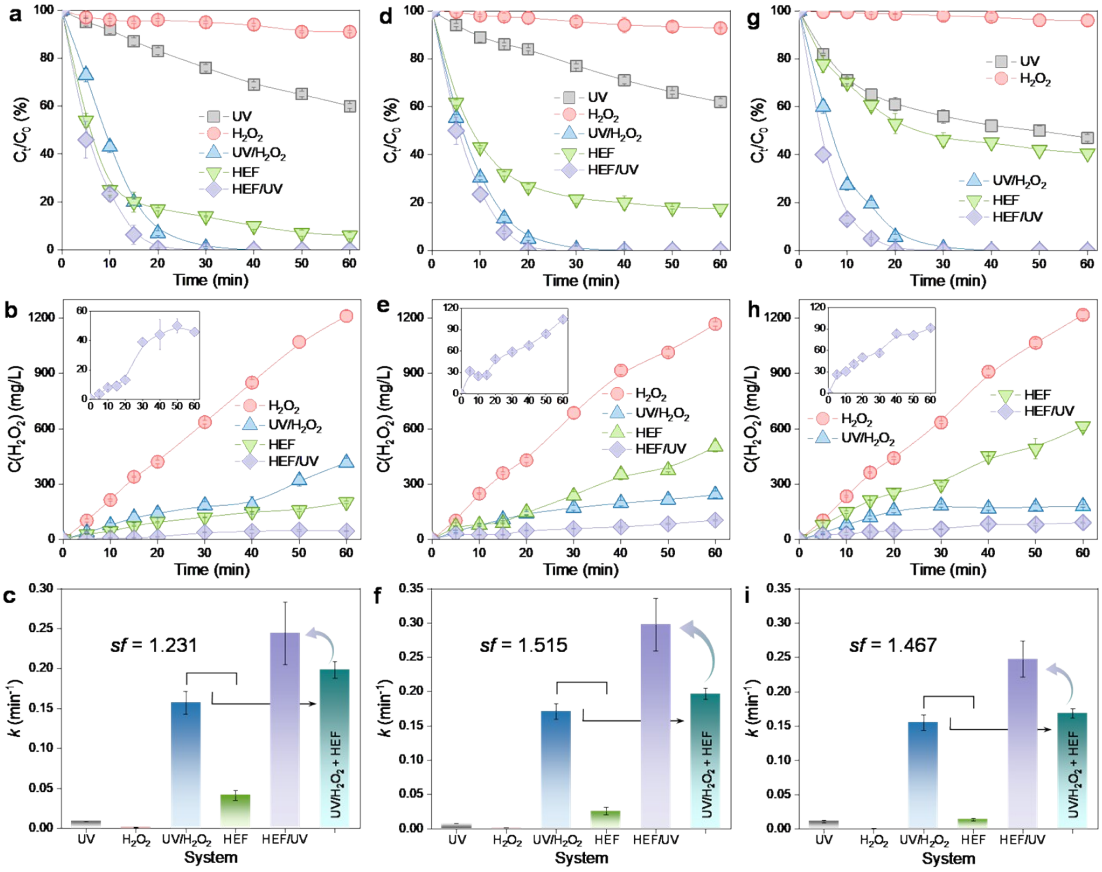

Fig. S10. Effect of different initial solution pH on process efficiency: (a–c) pH = 4, (d–f) pH = 6, and (g–i) pH = 8. OTC degradation performance in different systems (first row), corresponding H_2O_2 concentration evolution (second row), and comparison of apparent rate constant *k* (third row) (conditions: [OTC] = 20 mg/L, I_{ADC} = 100 mA/cm^2, $I_{FeOCl/GF}$ = 5 mA/cm^2, and UV = 6 W).

For the UV system, it can be observed that the degradation rate of OTC by direct photolysis gradually increases from 40.0% at pH 4 (Fig. S10a) to 53.6% at pH 8 (Fig. S10g), which may be related to the different predominant OTC species at different pH values. In fact, there are many dissociated forms of OTC at pH range of 3–8.5 (H_3OTC^+, H_2OTC, $HOTC^-$, and OTC^{2-}) with distinct physicochemical properties.[1] And OTC^{2-} was found to be the fastest degradable form for the photolysis followed

by $HOTC^-$, H_2OTC, and H_3OTC^+ by the increasing molar absorptivity at 254 nm,[2] which explained the accelerated degradation of OTC with increasing pH in the UV system. In contrast, the degradation kinetics of OTC in the HEF system showed a tendency to decrease with pH (0.04114 min^{-1} at pH 4 and 0.01373 min^{-1} at pH 8), which was because the alkaline microenvironment on the surface of the catalytic cathode aggravated the hydrolysis reaction of the active Fe center, thereby reducing the Fenton activity of the cathode to H_2O_2.[3] This is supported by the increase in the residual unactivated concentration of H_2O_2 in the HEF effluent from 201.8 mg/L at pH 4 (Fig. S10b) to 615.2 mg/L at pH 8 (Fig. S10h). In addition, an increase in solution alkalinity also resulted in decreased total iron leaching from the FeOCl/GF interface, which could attenuate the contribution of homogeneous EF (albeit weak overall) to the degradation of OTC, as demonstrated in Fig. S11.

Unlike both the HEF and UV systems, the best OTC degradation efficiency in the UV/H_2O_2 system was found to be achieved at pH 6. Alkaline media are well known to facilitate the formation of hydroperoxide anion (HO_2^-, a deprotonated form of H_2O_2) in H_2O_2 solution, which was reported to have higher molar absorptivity than H_2O_2 and therefore has the potential to produce more •OH under UV irradiation.[4] Indeed, the residual concentration of H_2O_2 in the UV/H_2O_2 system decreased from 416.4 mg/L at pH 4 (Fig. S10b) to 181.1 mg/L at pH 8 (Fig. S10h). Furthermore, as well established by Liu et al., the reactivity of different dissociated forms of OTC toward •OH follows the following order: OTC^{2-} > $HOTC^-$ > H_2OTC > H_3OTC^+ (i.e., increases with increasing pH).[1] Notwithstanding the above, an increase in pH

simultaneously leads to a significant decrease in the redox potential of •OH according to the Nernst equation (Eq. (S1)).[5] In addition, considering that •OH react with HO_2^- (Eq. (S2)) two orders of magnitude faster than with H_2O_2 (Eq.(11) in the main text),[1] the risk of •OH being scavenged by predominant HO_2^- at circumneutral and basic pH conditions will be increased. Taking these together, the *k* value was found to be highest at pH 6 for the UV/H_2O_2 system. Similarly, the HEF/UV tandem system also achieved optimal coupling and degradation efficiency at pH 6, which was considered to be a compromise between the different reaction characteristics of each subprocess in terms of initial solution pH.

$$E_{\bullet OH} = E^0_{\bullet OH} - 0.059pH \quad \text{(S1)}$$

$$HO_2^- + \bullet OH \rightarrow OH^- + HO_2^\bullet \quad k = 7.5 \times 10^9\ M^{-1}\ s^{-1} \quad \text{(S2)}$$

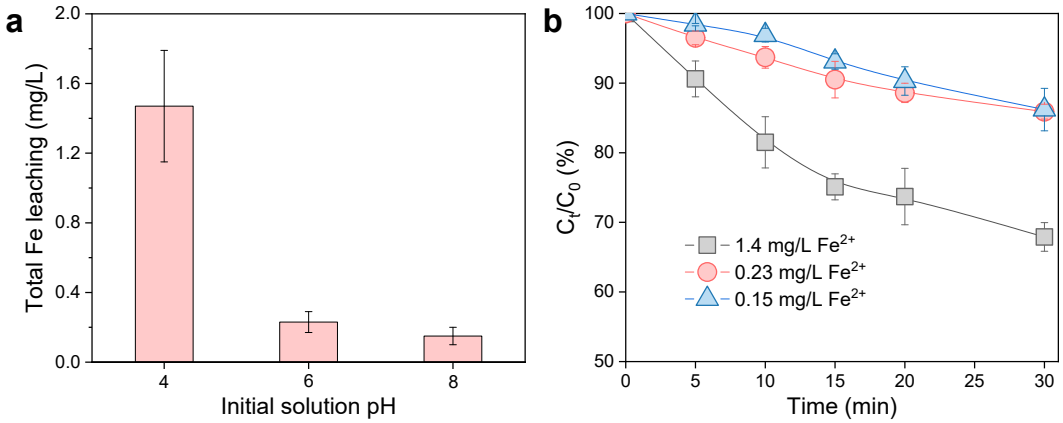

Fig. S11. (a) Concentration of total Fe leached from FeOCl/GF surface at different initial solution pH and (b) corresponding OTC degradation performance by induced homogeneous EF (conditions: ADC cathode, Ti/Pt mesh anode, [OTC] = 20 mg/L, and I_{ADC} = 100 mA/cm^2).

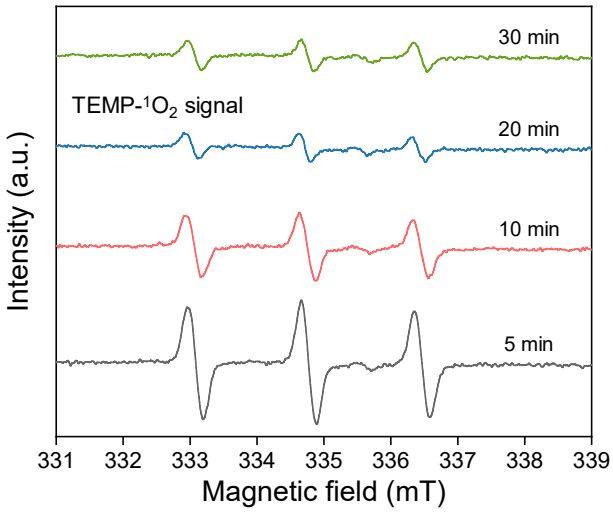

Fig. S12. Evolution of TEMP-$^1O_2$ signal intensity with reaction time in the HEF/UV tandem system.

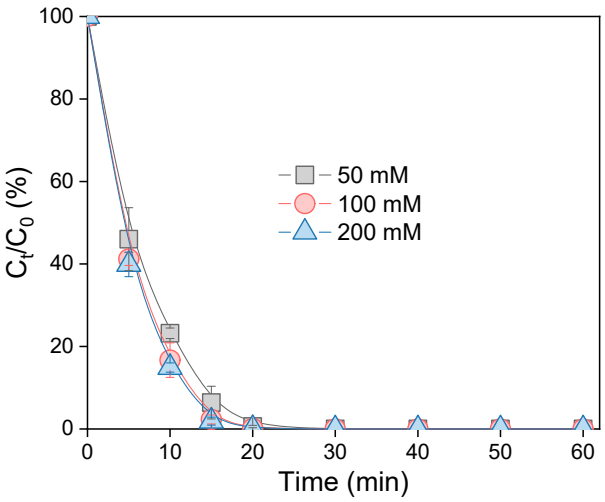

Fig. S13. Effect of different Na_2SO_4 electrolyte concentrations on OTC degradation (conditions: [OTC] = 20 mg/L, pH = 4, I_{ADC} = 100 mA/cm^2, $I_{FeOCl/GF}$ = 5 mA/cm^2, and UV = 6 W).

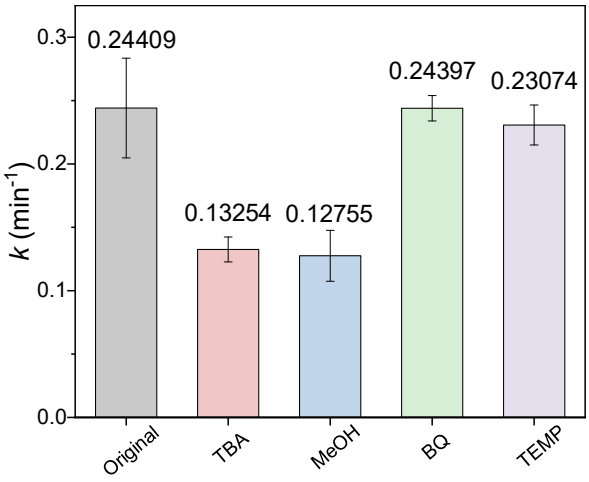

Fig. S14. OTC degradation in the presence of various quenching agents ([TBA] = 100 mM, [MeOH] = 100 mM, [BQ] = 2.5 mM, and [TEMP] = 1.0 mM).

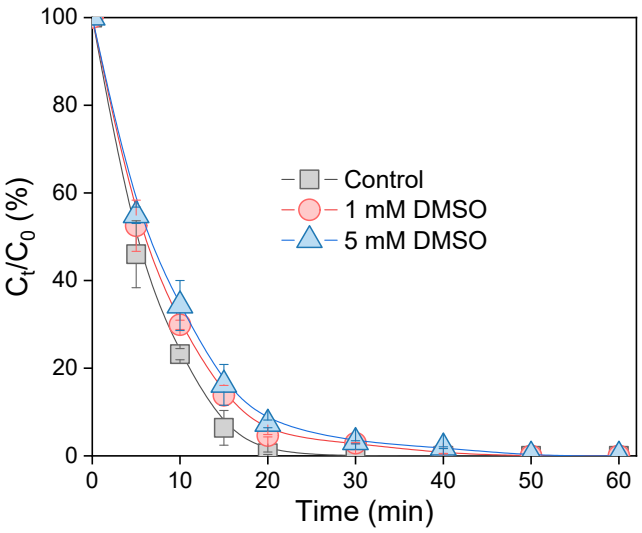

Fig. S15. Effect of DMSO concentration on OTC degradation in the dual-cathode HEF and UV tandem system.

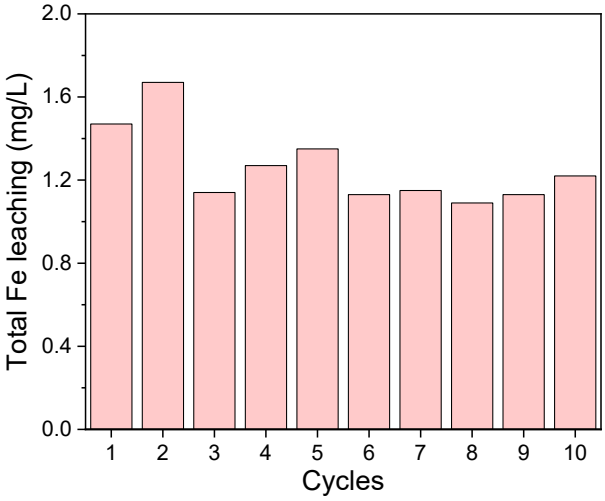

Fig. S16. Total Fe concentration leached from the FeOCl/GF catalytic cathode in the HEF/UV tandem system during 10 consecutive runs.

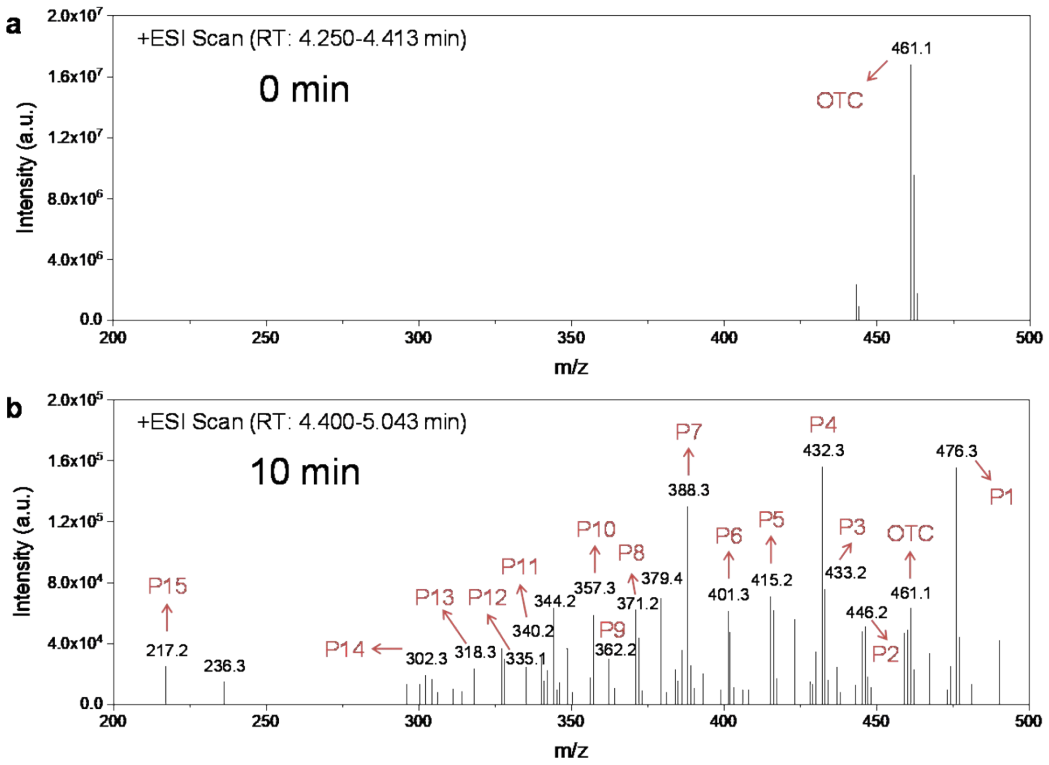

Fig. S17. MS spectra of intermediates detected during OTC degradation by the HEF/UV tandem system at different reaction times: (a) 0 min and (b) 10 min.

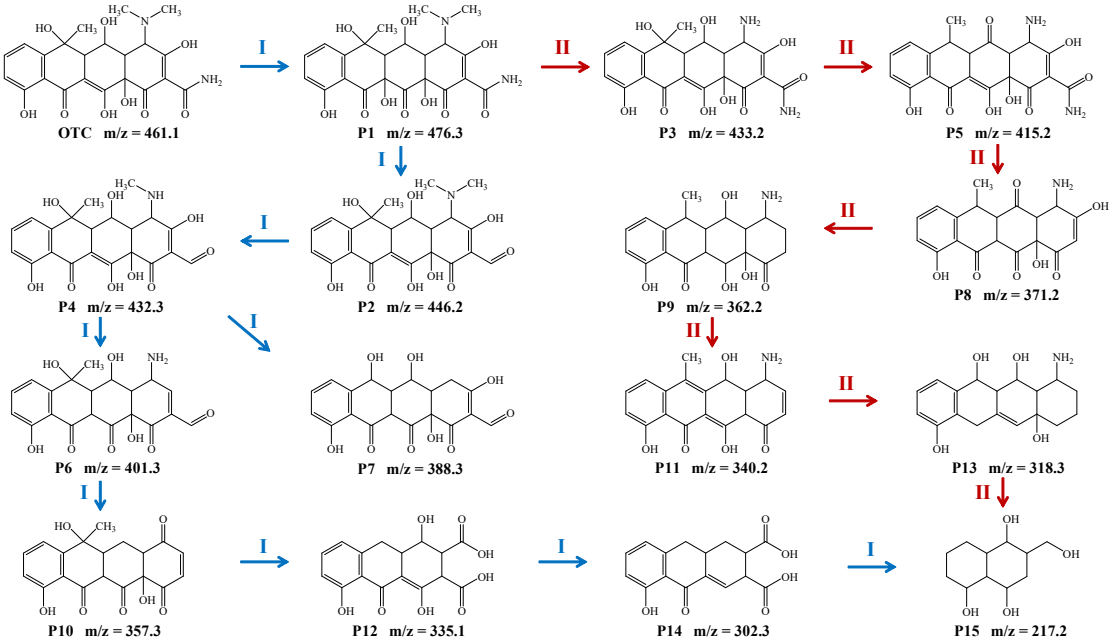

Fig. S18. Possible transformation pathways of OTC in the dual-cathode HEF and UV tandem system.

Table S1. Comparison of energy consumption for H_2O_2 production with literature.

Cathode	Electrolyte	Current density (mA/cm^2)	O_2 source	H_2O_2 yield ($mg/cm^2/h$)	CE (%)	EEC (kWh/kg)	Ref.
GDE	0.05 M Na_2SO_4	28.9	O_2 aeration	19.2	88.1	11.6	6
GDE	0.05 M Na_2SO_4	35.7	Air aeration	12.2	51−88	15.9	7
GDE	0.05 M Na_2SO_4	65	Air aeration	13.9	33.8	53.9	8
GDE	0.1 M K_2SO_4	-1.1 V vs. SCE	O_2 aeration	1.1	−	18.8	9
GDE	Solid electrolyte	3−50	Air aeration	1.8−20.3	79.1−58.4	3.7−34.6	10
INAC	0.1 M Na_2SO_4	14.3	Open air	6.5	~70	7.6	11
ABC	0.05 M Na_2SO_4	30	Open air	16.1	~80	10.4	12
GDE	0.1 M Na_2SO_4	-1.0 V vs. Ag/AgCl	O_2 aeration	5.1	57.3	7.2	13
GDE	0.05 M H_2SO_4	8	O_2 aeration	−	40	<8	14
ADC	0.05 M Na_2SO_4	5−100	Open air	3.3−54.1	85.3−100	5.3−44.2	This work

GDE: gas diffusion electrode; INAC: integrated natural air-diffusion cathode; ABC: air breathing cathode; ADC: air-diffusion cathode.

Table S2. Specific water quality parameters for different real water matrices.

Samples	Tap water	River water	Lake water
pH	7.04	6.82	6.91
COD (mg/L)	-	<15	<15
NH_3 (mg/L)	-	0.30	0.09
NO_3^- (mg/L)	1.40	2.73	0.11
PO_4^{3-} (mg/L)	-	0.01	<0.01
Cl^- (mg/L)	15.90	22.77	4.19
CO_3^{2-} (mg/L)	-	98.20	16.90
Conductivity (μS/cm)	182.80	356.00	47.20

Note: "-" means that the parameter was undetected or the concentration of the target parameter is below the detection limit. River water and lake water were collected from Dasha river of Shenzhen city and Tsinghua SIGS campus, respectively.

Table S3. Mass spectrometry information and structures of the possible intermediates.

Compounds	Formula	*m/z*	Proposed structure
OTC	$C_{22}H_{24}N_2O_9$	461.1	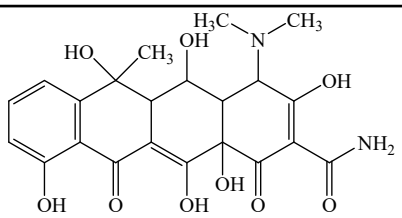
P1	$C_{22}H_{24}N_2O_{10}$	476.3	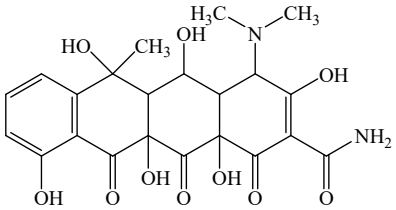
P2	$C_{22}H_{23}NO_9$	446.2	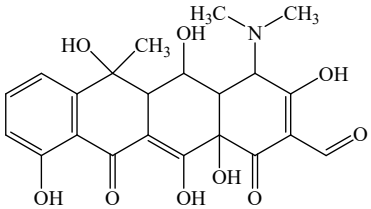
P3	$C_{20}H_{20}N_2O_9$	433.2	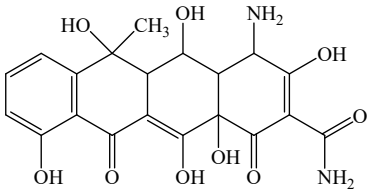
P4	$C_{21}H_{21}NO_9$	432.3	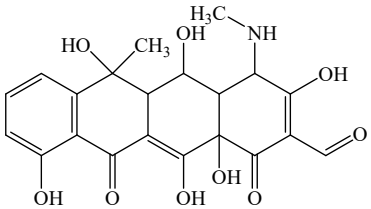
P5	$C_{20}H_{18}N_2O_8$	415.2	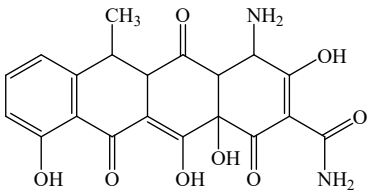
P6	$C_{20}H_{19}NO_8$	401.3	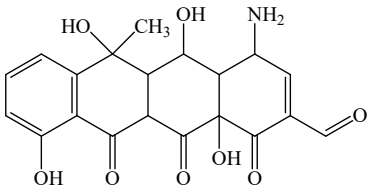

P7	$C_{19}H_{16}O_9$	388.3	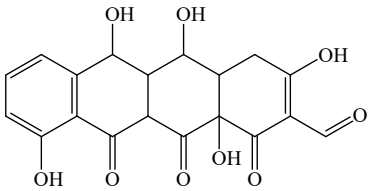
P8	$C_{19}H_{17}NO_7$	371.2	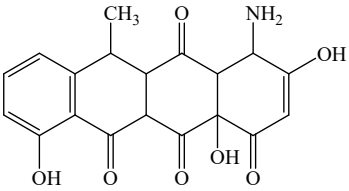
P9	$C_{19}H_{23}NO_6$	362.2	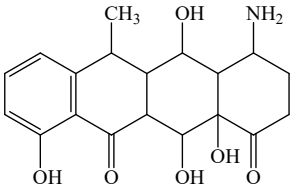
P10	$C_{19}H_{16}O_7$	357.3	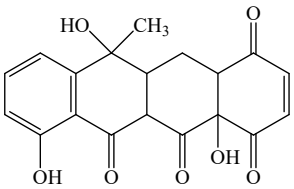
P11	$C_{19}H_{17}NO_5$	340.2	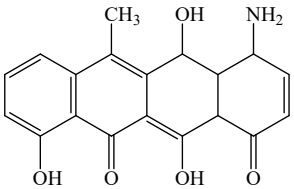
P12	$C_{16}H_{14}O_8$	335.1	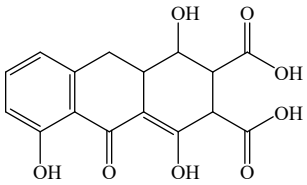
P13	$C_{18}H_{23}NO_4$	318.3	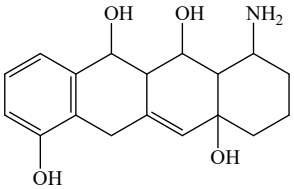

P14	$C_{16}H_{14}O_6$	302.3	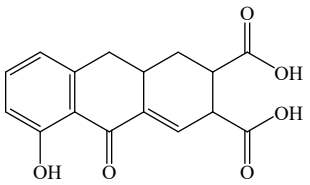
P15	$C_{11}H_{20}O_4$	217.2	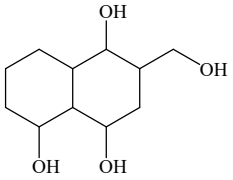

Table S4. Acute and chronic toxicity of OTC and its degradation intermediates predicted by ECOSAR software.

Compounds	Acute toxicity (mg/L)			Chronic toxicity (mg/L)			Hazard category
	Fish (LC_{50})	Daphnid (LC_{50})	Algae (EC_{50})	Fish (ChV)	Daphnid (ChV)	Algae (ChV)	
OTC	178	9.34	45.8	3.36	2.36	7.91	Toxic[a]
P1	60.7	3.04	8.35	0.466	0.666	1.30	Very toxic
P2	170	8.95	43.5	3.20	2.26	7.54	Toxic
P3	1.40×10^3	11.9	104	5.37	3.13	12.1	Toxic
P4	190	9.54	51.5	3.66	2.44	8.50	Toxic
P5	174	4.54	19.0	1.03	1.06	2.67	Toxic
P6	110	3.62	13.1	0.716	0.828	1.90	Very toxic
P7	1.02×10^3	452	93.5	96.4	42.7	392	Harmful
P8	35.6	2.08	5.17	0.290	0.449	0.826	Very toxic
P9	46.1	2.31	6.33	0.354	0.505	0.987	Very toxic
P10	6.33	4.80	1.48	0.832	0.679	7.36	Very toxic
P11	30.9	1.87	4.53	0.255	0.401	0.728	Very toxic
P12	168	520	18.3	160	53.0	141	Harmful
P13	56.5	2.36	7.28	0.403	0.526	1.10	Very toxic
P14	270	132	24	27.5	15.1	54.4	Harmful
P15	9.94×10^4	4.25×10^4	9.85×10^3	6.96×10^3	1.89×10^3	1.38×10^3	Not harmful

[a] The lowest of

acute toxicity values between and within the different trophic levels (fish, daphnid and algae) were used to define the appropriate hazard category of the compounds. According to the system established by the Globally Harmonized System of Classification and Labeling of Chemicals (GHS), the predicted toxicity values of TC and all intermediates can be divided into four categories: very toxic ($LC_{50}/EC_{50}/ChV < 1$ mg/L), toxic (1 mg/L $< LC_{50}/EC_{50}/ChV <$ 10 mg/L), harmful (10 mg/L $< LC_{50}/EC_{50}/ChV <$ 100 mg/L), and not harmful ($LC_{50}/EC_{50}/ChV > 100$ mg/L).

Table S5. Specific water quality parameters for real antibiotic wastewater.

TOC (mg/L)	pH	Conductivity (μS/cm)	SS (mg/L)	TN (mg/L)	NH_3-N (mg/L)	TDS (mg/L)
237	7.15	5030	226	78	18	3144

SS: suspended solids; TN: total nitrogen; TDS: total dissolved solids.

References

1. Y. Liu, X. He, X. Duan, Y. Fu and D. D. Dionysiou, *Chem. Eng. J.*, 2015, **276**, 113-121.
2. C. H. Han, H. D. Park, S. B. Kim, V. Yargeau, J. W. Choi, S. H. Lee and J. A. Park, *Water Res.*, 2020, **172**, 115514.
3. F. Deng, S. Li, Y. Cao, M. A. Fang, J. Qu, Z. Chen and S. Qiu, *J. Power Sources*, 2020, **466**, 228342.
4. S. Dhaka, R. Kumar, S.-h. Lee, M. B. Kurade and B.-H. Jeon, *J. Clean. Prod.*, 2018, **180**, 505-513.
5. Y. Q. Gao, J. Zhang, C. Li, F. X. Tian and N. Y. Gao, *Chemosphere*, 2020, **243**, 125325.
6. P. Ding, L. Cui, D. Li and W. Jing, *Ind. Eng. Chem. Res.*, 2019, **58**, 6925-6932.
7. X. Yu, M. Zhou, G. Ren and L. Ma, *Chem. Eng. J.*, 2015, **263**, 92-100.
8. I. Salmerón, K. V. Plakas, I. Sirés, I. Oller, M. I. Maldonado, A. J. Karabelas and S. Malato, *Appl. Catal. B Environ.*, 2019, **242**, 327-336.
9. J. F. Carneiro, R. S. Rocha, P. Hammer, R. Bertazzoli and M. R. V. Lanza, *Appl. Catal. A Gen.*, 2016, **517**, 161-167.
10. Y. Zhao, N. Deng, Z. Fan, Z. T. Hu, L. Fan, J. Zhou and X. Huang, *Chem. Eng. J.*, 2022, **430**, 132829.
11. S. Guo, M. Chen, Q. Zeng, J. E. Yang, J. Xie, Y. Wang and Q. Sun, *ACS EST Water*, 2022, **2**, 1647-1658.
12. S. Wang, D. Ye, X. Zhu, Y. Yang, J. Chen, Z. Liu, R. Chen and Q. Liao, *Sep. Purif. Technol.*, 2023, **305**, 122397.
13. L. Liang, M. Zhou, X. Lu, P. Su and J. Sun, *Electrochim. Acta*, 2019, **320**, 134569.
14. J. Filippi, H. A. Miller, L. Nasi, M. V. Pagliaro, A. Marchionni, M. Melchionna, P. Fornasiero and F. Vizza, *Mater. Today Energy*, 2022, **29**, 101092.